The Journal of Comparative Neurology 513:457–468 (2009)

Macromolecular Connections of Active Zone Material to Docked Synaptic Vesicles and Presynaptic Membrane at Neuromuscular Junctions of Mouse

SHARUNA NAGWANEY, MARK LEE HARLOW, JAE HOON JUNG, JOSEPH A. SZULE, DAVID RESS, JING XU, ROBERT M. MARSHALL, AND UEL JACKSON MCMAHAN*
Department of Neurobiology, Stanford University School of Medicine, Stanford, California 94305

ABSTRACT

Electron tomography was used to view macromolecules composing active zone material (AZM) in axon terminals at mouse neuromuscular junctions. Connections of the macromolecules to each other, to calcium channels in the presynaptic membrane, and to synaptic vesicles docked on the membrane prior to fusing with it during synaptic transmission were similar to those of AZM macromolecules at frog neuromuscular junctions previously examined by electron tomography and support the hypothesis that AZM regulates vesicle docking and fusion. A species difference in the arrangement of AZM relative to docked vesicles may help account for a greater vesicle-presynaptic membrane contact area during docking and a greater probability of fusion during synaptic transmission in mouse. Certain AZM macromolecules in mouse were connected to synaptic vesicles contacting the presynaptic membrane at sites where fusion does not occur. These secondary docked vesicles had a different relationship to the membrane and AZM macromolecules than primary docked vesicles, consistent with their having a different AZM-regulated behavior. J. Comp. Neurol. 513:457–468, 2009. © 2009 Wiley-Liss, Inc.

Indexing terms: active zones; neuromuscular junctions; synapses; vesicle docking; electron tomography

The active zones at the presynaptic plasma membrane of axon terminals, where initial events in impulse transmission take place at the nervous system's synapses, typically include three prominent structures: dense aggregates of cytoplasmic macromolecules called active zone material (AZM; also called membrane thickenings or presynaptic dense projections), which are attached to the membrane; synaptic vesicles docked on (i.e., held at) the membrane next to the AZM; and aggregates of macromolecules that include calcium channels within the membrane. The roles of docked synaptic vesicles and calcium channels in synaptic transmission are well understood: Depolarization of the presynaptic membrane by a nerve impulse causes the channels to open, allowing the entry of calcium into the terminal's cytoplasm, which triggers the protein-mediated fusion of docked vesicles with the membrane and exocytosis of the neurotransmitter they contain to act on the postsynaptic cell (Katz, 1969; Heuser and Reese, 1977). The function of the AZM, however, has only recently begun to be examined. Studies on the structural relationships of AZM macromolecules at the frog's neuromuscular junction (NMJ) by electron tomography (ET; also electron microscope tomography), which provides the best spatial resolution currently available for imaging structures in situ, together with biochemical studies on proteins implicated in vesicle docking and fusion have led to the hypothesis that the AZM is a multifunctional organelle that helps dock synaptic vesicles on the presynaptic membrane, anchors the calcium channels in the membrane at a particular distance from each other and the docked vesicles, and is involved in fusion of the vesicles with the membrane during synaptic transmission (Harlow et al., 2001; Südhof, 2004; see also Dresbach et al., 2001).

AZM varies considerably in size and in its position relative to docked vesicles from one synaptic type to another and even within the same synaptic type between animal species (Gray,

Grant sponsor: National Institute of Neurological Disorders and Stroke; Grant numbers: NS014506 and NS007158; Grant sponsor: National Institute of Mental Health; Grant number: Human Brain Project/Neuroinformatics, MH068065; Grant sponsor: postdoctoral fellowship from the National Sciences and Engineering Research Council of Canada (to J.A.S.).

The first two authors contributed equally to the study.

Present address for Sharuna Nagwaney: Bain & Co., Inc., London WC2N 5RW, United Kingdom.

Present address for David Ress: Imaging Research Center, University of Texas, Austin, TX 78759.

Present address for Jing Xu: Merck & Co., Inc., Rahway, NJ 07065.

*Correspondence to: U.J. McMahan, Department of Neurobiology, Stanford University School of Medicine, Fairchild D200, 299 Campus Dr., Stanford, CA 94305. E-mail: grantser@stanford.edu

Received 30 May 2008; Revised 7 October 2008; Accepted 16 December 2008

DOI 10.1002/cne.21975

Published online in Wiley InterScience (www.interscience.wiley.com).

1966; Couteaux and Pécot-Dechavassine, 1970; Peters et al., 1991). Accordingly, an essential test of the hypothesis concerning AZM function based on the ET studies of the active zone at the frog's NMJ is the identification of comparable relationships between AZM macromolecules, docked vesicles, and presynaptic membrane macromolecules at synapses where the active zones have a different gross topography from that at frog NMJs. The aim of the study reported here was to determine by ET whether there were such relationships at NMJs of mouse muscles (*levator auris*), where the active zones are significantly smaller and the AZM has a markedly different distribution relative to docked vesicles than at frog NMJs. Such an analysis on synapses in the mouse is also of interest because of the greater availability of methods for localizing known synaptic proteins in mammals (e.g., Südhof, 2004; Takamori et al., 2006), which could be helpful in understanding the protein composition of the AZM macromolecules and, thus, provide additional tests of the hypotheses.

MATERIALS AND METHODS

Preparation

The bilaterally paired *levator auris* muscles (Angaut-Petit et al., 1987), which lie just beneath the skin, are broad but only a few muscle fibers thick. They were exposed in four terminally anesthetized (50 mg/kg pentobarbital, intraperitoneally; Sigma, St. Louis, MO) mice (C57/BL6) under a dissecting microscope. Mouse Ringer's solution (150 mM NaCl, 5.6 mM KCl, 2.25 mM $CaCl_2$, 2.4 mM $NaHCO_3$, 0.56 mM glucose, pH adjusted to 7.2 with NaOH) containing tetrodotoxin (10 mg/mL; Sigma) was dripped onto the muscles' superficial surface and injected next to their deep surface for 10 minutes to inhibit impulse evoked synaptic activity that might be caused by the application of fixative. The fixative, a solution of 1% glutaraldehyde (Ted Pella, Redding, CA) in Millonig's phosphate buffer (PB), which was isosmolar to the Ringer's solution (320 mOsM total, pH 7.2), was applied similarly for 30 minutes. The muscles were then removed from the animal and pinned out flat in Sylgard 184 (Dow Corning, Midland, MI)-coated Petri dishes containing the same fixative for 30 minutes. They were washed for 1 hour in 320 mOsM PB (pH 7.2), fixed, and stained for 1 hour in 1% OsO_4 in PB (pH 7.2), washed 1 hour in H_2O, stained 1 hour in saturated aqueous uranyl acetate, dehydrated in increasing concentrations of ethanol, and embedded flat in a wafer of Eponate 12 (Ted Pella) less than 1 mm thick. Regions of the muscles containing NMJs were identified in the wafers at 400× magnification with a light microscope, and blocks containing them were cut out and mounted for sectioning. The sections varied from 50–250 nm in thickness. They were stained with uranyl acetate in methanol and with aqueous lead citrate.

In ET studies on active zones in axon terminals of frog NMJs fixed either with an isosmolar solution of 1% glutaraldehyde in Millonig's PB (220 mOsM total) or by ultrarapid freezing (Heuser and Reese, 1981), which is preferable for characterizing the structure of certain cellular components, we observed no significant difference in the diameter of synaptic vesicles, in the presence of beams, ribs, and pegs in the AZM, and in the spacing between the pegs (unpubl. obs.; see also Sosinsky et al., 2008). We chose to use glutaraldehyde fixation for the experiments presented here because of its convenience.

The animal experimentation described here was approved by Stanford University's Administrative Panel on Laboratory Animal Care (IACUC), which oversees the use of animals according to U.S. federal law.

Data collection

Datasets were collected at 23,000× to 59,000× magnification with an FEI Polara G2 TEM electron microscope (FEI, Hillsboro, OR) equipped with a 2048 × 2048 CCD (Tietz F224HD; Tietz Video and Imaging Processing Systems, Gauting, Germany) in this laboratory or at 31,000× with a Phillips Tecnai T20 electron microscope (FEI) equipped with a 1024 × 1024 CCD (Gatan, Pleasanton, CA) in the laboratory of Dr. David Agard at the University of California, San Francisco, using an automatic data acquisition procedure (UCSF Tomography; Zheng et al., 2004). The stage was cooled to liquid nitrogen temperature to reduce specimen shrinkage. Eight of the 13 datasets used for this study consisted of images taken at 1-degree tilt intervals to ±60 or ±70 degrees along a single tilt axis. The remaining five datasets consisted of images taken at 1-degree intervals to ±60 degrees along each of two orthogonal tilt axes. Reconstructions from the dual axis datasets have less noise than those made from single axis datasets (Penczek et al., 1995; Cristina et al., 2005). However, both types of datasets yielded qualitatively similar structural models of AZM components, and measurements from both types rose to statistical significance.

For generating reconstructions the images were first aligned automatically using 5 or 10 nm gold colloid (British Biocell International, Cardiff, UK) deposited on one or both sides of the sections before data collection. The average alignment error was 1.3 pixels (range, 0.9–2.2) root mean square. The reconstructions were made by a weighted back-projection method. Both the alignment and reconstruction algorithms are in the unified software package EM3D (Ress et al., 1999, 2004; http://em3d.org). The spatial resolution in reconstructions generated from datasets collected at 31,000× to 62,000× magnification, which were used for making the surface models, was 2–3 nm for high-contrast structures such as the cytoplasmic and extracellular layers of the plasma membrane (Ress et al., 1999).

Virtual slices, segmentation, and surface models

Virtual slices through the reconstructed tissue sections were 1 voxel thick. Depending on the magnification of the images in a dataset, the virtual slice thickness represented 0.58–1.5 nm of the tissue section's thickness. When necessary, the angular orientation of the slice plane was adjusted to maximize contrast boundary discrimination of the structures under study.

Structures were segmented from the high-resolution reconstructions (1 voxel = 0.58–1.16 nm) by using a combination of manual and semiautomatic methods in EM3D to define individual volumes-of-interest (VOIs; Ress et al., 2004). For the presynaptic membrane and synaptic vesicles, which were heavily stained and had a simple geometry, a semiautomatic scheme was used. For structures that had a complex geometry and light to moderate stain, VOIs were defined by manually marking a closed path on a series of slices. The VOIs were slightly larger than the structures that they enclosed to allow accurate and complete isodensity-surface calculations for the surface models.

We used EM3D to calculate and render a surface model for each VOI. The calculation was done using a gray scale value that minimized the mean spatial uncertainty averaged across the whole area of the model. Surface models generated in this way had a spatial resolution equal to the resolution of the reconstructed volumes (Ress et al., 2003, 2004).

Surface models were generated from nine reconstructions (four single tilt-axis and five double tilt-axis datasets) from both of the *levator auris* muscles in one mouse. Serial virtual slices through these reconstructions were also examined in detail. Structural relationships quantitatively characterized in the surface models and serial slices from the one mouse were checked by eye in serial virtual slices from reconstructions (four single tilt-axis datasets) made from the muscles taken from three other mice. In all cases the relationships of primary docked vesicles, secondary docked vesicles, and invaginations in the presynaptic membrane to AZM, in general, and to the AZM's ribs, beams, and pegs, in particular, was similar.

Contact areas between docked vesicles and presynaptic membrane

In order to measure the size of the area of contact between the membrane of docked synaptic vesicles and the presynaptic plasma membrane at an active zone, surface models of each were first generated using EM3D (Ress et al., 2004). The distance between each polygon vertex on the presynaptic membrane model and synaptic vesicle model was then computed. The area where the distance between them was within a spatial tolerance of 1.5 nm, which was below the resolution of the reconstructed volumes, was considered the contact area. To determine the size of the contact area it was projected onto a best-fit plane using the Pearson's eigenvalues method (Pearson, 1901). Briefly, a matrix containing the coordinates of vertices in the contact region was generated and the centroid of the contact region was subtracted from the matrix. The matrix was transposed and multiplied by the original producing a 3 × 3 covariant matrix. After obtaining the covariance matrix of vertices comprising the contact region, eigenvectors and eigenvalues were computed (Arfken, 1985). The eigenvector corresponding to the smallest eigenvalue of the covariance matrix was considered the normal vector to the best-fit plane passing through the centroid of the contact region. Subsequently, the area of the projected contact region on the best-fit plane was calculated.

Diameter of docked vesicles

Serial virtual slices made through reconstructed volumes in their x-y plane were used to identify the slice for each vesicle that passed through its equator. Because the vesicles were not perfect spheres, diameters to the outer surface of the vesicle membrane were measured for each vesicle along four separate axes (≈45° increments) and expressed as an average.

Figure preparation

Figure layouts were prepared using Adobe Photoshop CS3 (Adobe Systems, San Jose, CA) without manipulation except for Figure 7D. For the reproduction shown in Figure 7D, brightness and contrast were adjusted and an arrowhead was removed using Adobe Photoshop CS3.

RESULTS

Gross topography of active zones

The layout of the active zone at NMJs of mouse and other mammals has been best characterized by analysis of replicas of freeze-fractured presynaptic membranes imaged by conventional two dimensional (2D) electron microscopy (Rash and Ellisman, 1974; Ellisman et al., 1976; Fukunaga et al., 1982, 1983; Fukuoka et al., 1987). Here, each active zone is represented by two nearly parallel "double rows" of membrane macromolecules 10–12 nm in diameter. The paired double rows of macromolecules are situated directly opposite infoldings (junctional folds) in the postsynaptic plasma membrane of the muscle fiber, and their long axis is orthogonal to the long axis of the mouths of the folds. Paired double rows of membrane macromolecules are also found at the active zones of NMJs in frog and on phasic muscle fibers in the lizard (Heuser and Reese, 1974; Walrond and Reese 1985; Pawson et al., 1998). In mouse the rows are about 80 nm long (Fukuoka et al., 1987), but both double rows of a pair are not always equal in length and, even when equal in length, they are not always in register (see fig. 2 in Fukuoka et al., 1987, which is in part reproduced here in Fig. 7D). The double rows of macromolecules in mouse have been shown to include calcium channels (Lang et al., 1987; Nagel et al., 1988). Because there is evidence that the double rows of macromolecules at active zones of frog NMJs include calcium activated potassium channels in addition to calcium channels, (Robitaille et al., 1993) and both types of channels must be in close proximity for normal synaptic function (Roberts et al., 1990), it is likely that both types are among the double rows at mammalian NMJs. Deformations in the presynaptic membrane indicative of vesicle fusion sites occur between the two double rows of macromolecules at rat and lizard NMJs exposed to a high potassium concentration, which causes exocytosis of neurotransmitter (Ellisman et al., 1976; Walrond and Reese, 1985), indicating that prior to fusion vesicles are docked on the cytoplasmic surface of the membrane between the double rows. The small size of the active zone at mammalian and lizard NMJs, however, has made it difficult to characterize directly the gross arrangement of vesicles and AZM by 2D electron microscopy on tissue sections. The greatest dimension of the active zone in the plane of the membrane is little more than the thickness of a routine tissue section (50–100 nm) and, because sections are cut from NMJs without knowledge of the position or orientation of active zones within them, in most cases only portions of active zones are included in sections and they occupy only a fraction of the section's depth. Thus, in 2D images of tissue sections the AZM, synaptic vesicles and cytoplasmic elements around the active zone partially obscure one another by overlap in the sections' depth axis. Nevertheless, studies on NMJs in rat led to the suggestion that vesicles at active zones are "nested" in the AZM (Ellisman et al., 1976).

ET on tissue sections makes it possible to reconstruct the sections in three dimensions (3D). Components of active zones can then be studied in virtual slices through the reconstructed volume many times thinner than the tissue section or, after segmentation from the volume, in 3D surface models (Harlow et al., 2001). Accordingly, structures at active zones can be observed in much greater detail by ET than by conventional 2D electron microscopy. We used tissue sections

50–250 nm thick from mouse muscles. The thicker tissue sections favored inclusion of entire active zones; the thinner sections provided better spatial resolution, making them useful for examining details of specific portions of active zones. Each of eight active zones that were entirely within our sections had two bands of AZM (Figs. 1, 2). Both bands were nearly rectangular in the plane of the presynaptic membrane, and they were nearly parallel to each other along their long axis. However, like the paired double rows of macromolecules, they were not always equal in length and, when equal in length, they were not always in register (Figs. 1D, 2). Both bands also consisted of an aggregate of filamentous macromolecules (Figs. 1B,C, 3A–D). The most compact region extended 50–60 nm from the cytoplasmic surface of the presynaptic membrane into the cytoplasm, but some of the filaments extended several tens of nanometers further to contact vesicles distal to the presynaptic membrane (Fig. 3D). There were no direct connections between the macromolecules in one band with those of the other at an active zone. However, between the pair of AZM bands there were two juxtaposed synaptic vesicles, which were aligned parallel to the bands' long axes. Both vesicles were connected to AZM macromolecules and they were in contact with the presynaptic membrane (Figs. 1B–D, 2, 3E,F). In most cases the membranes of the two vesicles were so close to each other that a space could not be resolved between them, but at two active zones there was a 3-nm and 10-nm gap between the membranes. The gap was bridged by one or two macromolecules ≈25 nm from the presynaptic membrane (Fig. 3E).

To estimate the position of the AZM bands and the pair of vesicles between them as seen in our 3D reconstructions relative to the double rows of macromolecules in the presynaptic membrane as seen in freeze-fracture replicas, we generated from our reconstructions of the eight complete active zones "area models" of the bands of AZM, which encompassed the boundaries of the bands in the vicinity of the presynaptic membrane (Fig. 2). We used the models to measure the dimensions of the bands and the distance between their midlines, and to determine the bands' orientation with respect to the mouths of the junctional folds in the postsynaptic membrane for comparison to the length, width, spacing, and orientation of the double rows of membrane macromolecules. Because the bands were not perfect rectangles in the plane of the presynaptic membrane (Fig. 1D), we first established by using serial virtual slices through the eight active zones an averaged length and width for each AZM band. This was done by measuring the bands from side-to-side and end-to-end at multiple points along each axis within 15 nm of the membrane. Averaging the measurements along each axis provided rectangular area models of the AZM bands in the plane of the presynaptic membrane, the edges of which were within ±10 nm of the true edges of the AZM bands. We then calculated the average length and width of the 16 area models to be 72 ± 19 nm (SD) and 27 ± 9 nm (SD), respectively. The average distance between the midlines of the models for the eight active zones was 56.8 ± 4.2 nm (SD). Serial virtual slices were also used to learn that each of the eight active zones was directly opposite a junctional fold in the postsynaptic membrane and that the long axis of the AZM bands was orthogonal to the long axis of the mouth of the fold (Figs. 2, 3E,F). We conclude that each band of AZM directly overlies a double row of membrane macromolecules throughout its length because: 1) The length and width of the double rows of membrane macromolecules as seen in freeze-fracture replicas is on average ≈80 nm and ≈30 nm, respectively (Fukuoka et al., 1987), which is similar to the average length and width of our AZM area models; 2) The distance between the midlines of the double rows is ≈60 nm (calculated from measurements in Fukuoka et al., 1987), which is similar to the distance between the midlines of the AZM area models; and 3) The long axis of the double rows is orthogonal to the long axis of the mouths of the apposing junctional folds in the postsynaptic membrane (Ellisman et al., 1976), as is the long axis of the AZM area models. This conclusion is confirmed by the correlation of the frequency and distribution of connections between AZM macromolecules and the presynaptic membrane and the frequency and distribution of membrane macromolecules in the double rows as described below. Because vesicle fusion sites are seen between the double rows in freeze-fracture replicas of the presynaptic membrane at activated rat and lizard NMJs (Ellisman et al., 1976; Walrond and Reese, 1985), which are similar to those of mouse, we also conclude that the two synaptic vesicles between and connected to the bands of AZM are docked on the presynaptic membrane prior to fusion with it during synaptic transmission.

There were up to three synaptic vesicles at active zones that were in contact with the presynaptic membrane at the ends of AZM bands, one vesicle per end, and each of these vesicles was connected to macromolecules in the AZM (Figs. 1D, 2, 3D). Because of the presence of such vesicles at the ends of the bands at all active zones in our sample (Fig. 2) and the fact that in our sections there were no vesicles in contact with the presynaptic membrane in the vast areas beyond the active zones, we conclude that these vesicles are selectively docked on (held at) presynaptic membrane at active zones as are those between the AZM bands. Each vesicle at the end of a band must be positioned just beyond the end of one of the double rows of macromolecules in the presynaptic membrane. However, freeze-fracture replicas of the presynaptic membrane at rat and lizard NMJs exposed to a high potassium concentration do not show membrane deformations characteristic of vesicle fusion at these sites (Ellisman et al., 1976; Walrond and Reese, 1985), which makes it likely that the docked vesicles at the ends of the bands in mouse have a different behavior from those between the bands. Thus, we refer to the vesicles between the bands of AZM as primary docked vesicles and the vesicles at the ends of the bands as secondary docked vesicles.

The primary docked vesicles were similar in appearance to secondary docked vesicles and to most undocked vesicles; their diameter was on average 55.6 ± 3.3 nm (SD; primary docked vesicles, n = 14; secondary docked vesicles, n = 9). At the site of closest apposition between the vesicle membrane and the presynaptic membrane there was no discernible space between the membranes (Fig. 3B,C,E,F). We did not seek to determine as part of this study whether the vesicle membrane and presynaptic membrane were "hemifused" as reported for the relationship of docked vesicles to presynaptic membrane in the rat CNS (Zampighi et al., 2006). When such sites for the primary docked vesicles were mapped on surface models of the presynaptic membrane they occupied an ovoid area (Fig. 4), which, on average, was 395 ± 40 nm^2 (SEM, n =

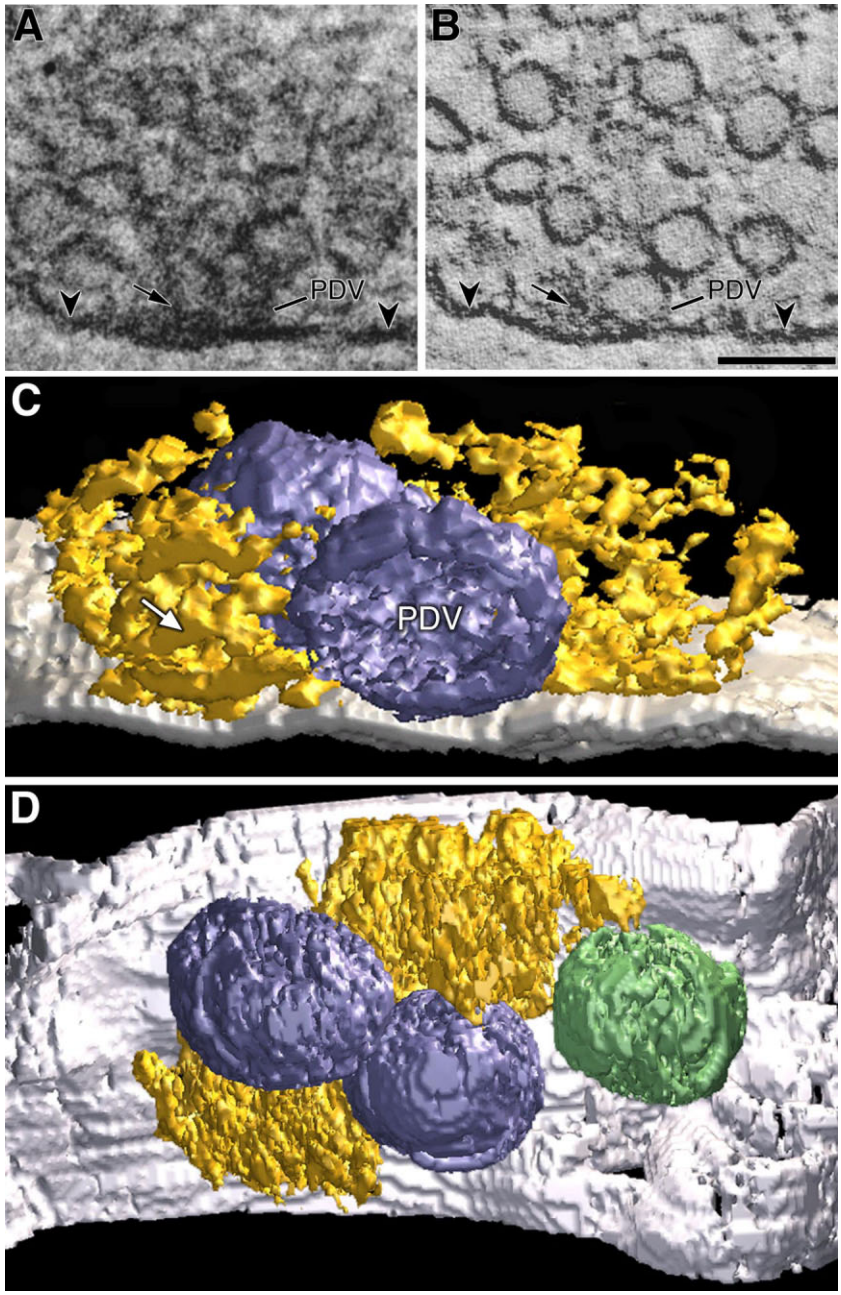

Figure 1.
Electron tomography on tissue sections from mouse neuromuscular junctions provides details of the active zone's gross topography not apparent in conventional electron micrographs. **A:** 2D image obtained by conventional electron microscopy of a portion of an axon terminal containing an active zone in a 50 nm thick tissue section. A patch of active zone material (AZM) (small arrow) attached to the presynaptic membrane (arrowheads) is partially overlapped by synaptic vesicles, one of which is a primary docked vesicle (PDV). **B:** 2D image of a virtual slice from near the surface of a volume reconstruction of the section imaged in A showing the same active zone. The patch of AZM (small arrow) is composed of filamentous macromolecules. The same PDV labeled in A is seen here to be connected to an AZM macromolecule on its lower left quadrant and to be in contact with the presynaptic membrane (arrowheads). **C:** 3D surface model of the active zone shown in A and B that was generated by segmentation of individual structures from the volume reconstruction using serial virtual slices including that in B. The AZM (gold) is arranged in two nearly parallel bands on the presynaptic membrane (white), one of which (small arrow) corresponds to the patch evident in A and B. A pair of PDVs (blue), one of which (PDV) is apparent in A and B, lies between the bands. The thickness of the tissue section did not include the ends of the active zone. **D:** Surface model of an entire active zone viewed horizontal to the presynaptic membrane. The active zone was taken from a thicker tissue section than the one used for A–C and shows the full extent of two bands of AZM (gold) on the presynaptic membrane (white), a pair of PDVs between the bands (blue), and a secondary docked vesicle (green) at the end of a band. The color code used here for AZM, primary and secondary docked vesicles and presynaptic membrane is the same for all figures except where noted. As referred to in subsequent figures a median plane of an active zone is orthogonal to the presynaptic membrane and parallel to the axis of the paired PDVs. A transverse plane is orthogonal to both the presynaptic membrane and the axis of the paired PDVs. A horizontal plane is parallel to the presynaptic membrane. Scale bar = 100 nm in B (applies to A).

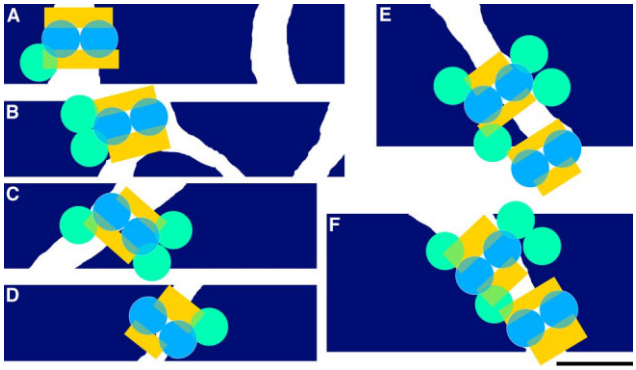

Figure 2.
Maps of the complete active zones in our samples showing the relationship of active zone material (AZM) bands to each other and to docked vesicles and the orientation of the bands relative to the mouths of junctional folds in the postsynaptic plasma membrane of the apposing muscle fibers. **A–F:** There is a pair of AZM bands at each active zone. The bands at an active zone are nearly parallel, but they can vary in length (C–E) and width, and even when similar in length they can be out of register (D). For all of the active zones there is a pair of juxtaposed primary docked vesicles between the AZM bands, and one or more secondary docked vesicles each of which is situated at the end of a band. For all of the active zones the long axis of the AZM bands is orthogonal to the long axis of the mouths of the junctional folds (white gap) in the postsynaptic membrane (dark blue). The maps were generated by projecting the different components onto a plane horizontal to the presynaptic membrane. The size and shape of the AZM bands were modeled as described in the text. The size and shape of the primary and secondary docked vesicles were modeled by creating circles around the center of each having a diameter equal to the average diameter of docked vesicles. Scale bar = 100 nm.

12). Similar maps of the site of contact between secondary docked vesicles and the presynaptic membrane also revealed an ovoid contact area (Fig. 4), but it was 187 ± 30 nm^2 (SEM, n = 10), which is significantly different ($P < 0.001$, two-tailed *t*-test) from the size of the contact area between primary docked vesicles and presynaptic membrane.

The presynaptic membrane between the AZM bands was nearly flat or smoothly curved (Fig. 3E,F). However, its contour just beyond the ends of the AZM bands was highly irregular; typically, in virtual slices there were profiles of invaginations in the membrane in line with the docked vesicles (Fig. 3E,F). We examined vast stretches of presynaptic membrane away from the AZM bands in serial virtual slices through our samples containing active zones, but we observed no such invaginations in the membrane more than 80 nm beyond the ends of the bands. We also observed in the serial virtual slices that just beyond those ends of AZM bands lacking secondary docked vesicles there were profiles of vesicles within 30 nm of the presynaptic membrane (Fig. 3D). They were in every case connected to macromolecules of the adjacent AZM band. Vesicles within 30 nm of the presynaptic membrane were found nowhere else in the terminals, either alongside the AZM bands or in association with the areas of presynaptic membrane further than 80 nm beyond the ends of AZM bands. Thus, the region of the axon terminal just beyond the ends of the AZM bands is specialized not only by the presence of secondary docked vesicles attached to the AZM, but also by deep presynaptic membrane invaginations and by undocked vesicles in unusually close proximity to the presynaptic membrane.

Connections of AZM macromolecules

Filamentous macromolecules arising from each band of AZM at an active zone terminated on the hemisphere of each of the primary docked vesicles facing it (Figs. 1C, 3A–C, 5). For each of 12 primary docked vesicles there were about 11 (10.5 ± 1.9, SD) AZM filament connection sites nearly equally distributed between the two hemispheres. Docked vesicles also had filamentous connections to nearby undocked vesicles similar to those that occur between undocked vesicles throughout axon terminals (Landis et al., 1988; Hirokawa et al., 1989; Siksou et al., 2007); we did not examine them as part of this study.

Within 15 nm of the presynaptic membrane there was a set of AZM macromolecules which, based on their connections and orientation relative to each other, to primary docked vesicles and to the presynaptic membrane, corresponded to beams, ribs, and pegs (Figs. 3A–D, 6, 7) identified in the same region of AZM at the frog's NMJ. There were five or six ribs in each AZM band at six complete active zones and in two bands from tissue sections that included only half of an active zone sectioned in the median plane of AZM (Figs. 3D, 6). One end of each rib was connected to a primary docked vesicle while the other end was connected to a beam. Each primary docked vesicle (n = 12) was connected to two or three ribs from each band, so that it had a total of five or six rib-vesicle connections from both bands. As reported for docked vesicles at frog NMJs (Harlow et al., 2001), there was often a slight protrusion in the vesicle membrane toward the AZM macromolecules, including ribs (Fig. 3B,C), at their sites of contact. A quantitative study on sites of contact between macromolecular filaments and undocked vesicles at frog NMJs fixed either by ultrarapid freezing (Heuser and Reese, 1981) or by glutaraldehyde, as used here, has shown that protrusions in the curvature of the vesicle membrane preferentially occur at the sites of contact (Xu and McMahan, unpubl. obs.). They would be expected if the macromolecules were connected to the vesicle membrane and exerted an outward force on it at the time of fixation. Using the proximity measurement tool in EM3D we determined the length of a straight line from the centroids of the rib-vesicle connection sites on 12 primary docked vesicles to the closest points on the presynaptic membrane. It was 8.5 ± 3.5 nm (SD, n = 42), which is similar to the result of comparable measurements made at active zones of frog NMJs (Ress et al., 2004). From their connection points on the vesicle, the ribs arced toward the membrane and then lay 2–4 nm from the membrane to where they connected to beams (Fig. 3A–C).

Beams were positioned at the edge of each AZM band distal to the primary docked vesicles (Figs. 3B,C, 6). In all of nine cases the beams were in contact with the presynaptic membrane, but in some cases they were up to 3 nm from the membrane over short stretches. They ran the full length of the band of AZM nearly orthogonal to the ribs, and the rib-beam connections were distributed serially. We discerned in each of three bands two beams lying in series and apparently connected to each other (Fig. 6D,E). The two beams were similar in length. The members of a pair were distinguished by slight differences in diameter (Fig. 6D). Moreover, at the point of connection there were both a narrow superficial crevasse and a short region of overlap (Fig. 6E) as observed for beam-beam connections in frog (Harlow et al., 2001).

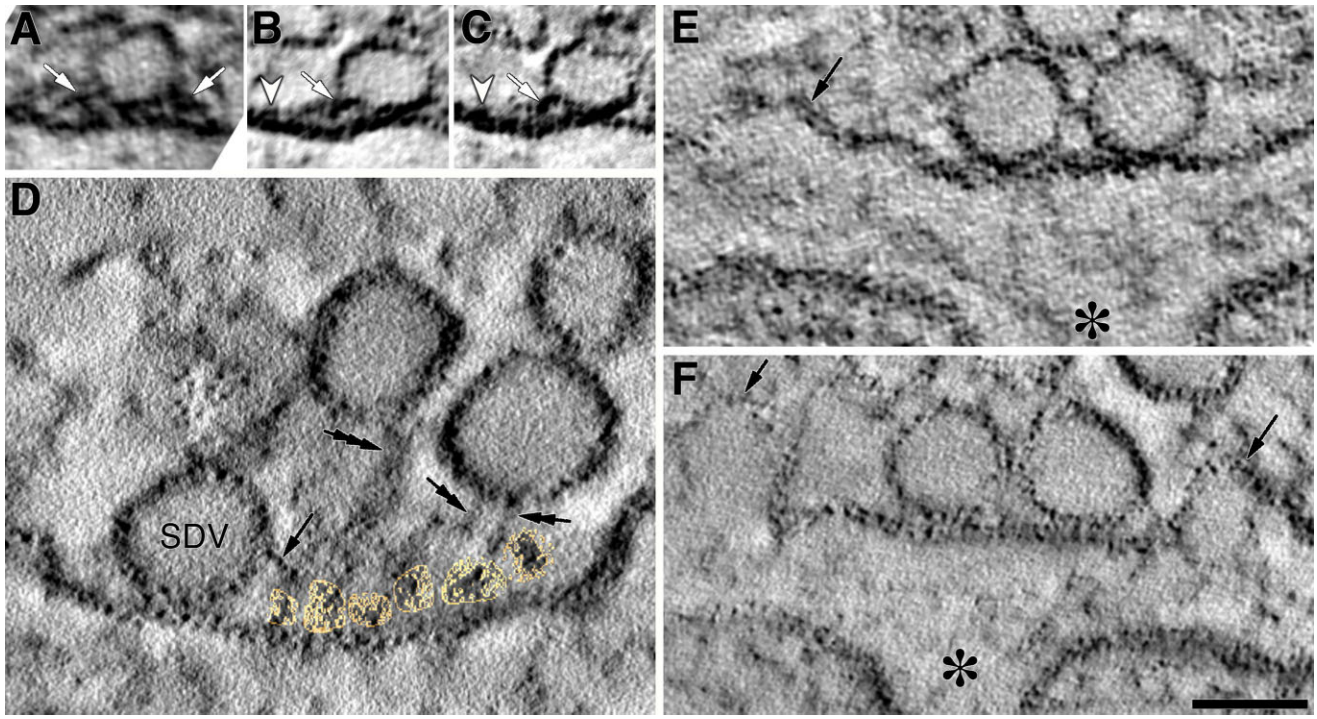

Figure 3.
Associations of primary and secondary docked vesicles with active zone material (AZM) and the presynaptic membrane as seen in virtual slices. **A:** A slice through the same primary docked vesicle shown in Figure 1A–C made in the transverse plane of the active zone. The vesicle is flanked by filamentous macromolecules of AZM bands including ribs (arrows). A peg extends from the left rib to the presynaptic membrane just opposite the arrow. **B,C:** Successive slices from a primary docked vesicle made near the transverse plane of an active zone showing portions of a rib (small arrow) and a beam (arrowhead). A peg extends from the left rib to the presynaptic membrane just opposite the arrow. The curvature of the vesicle is distorted toward the rib at its site of attachment. **D:** A slice made through an AZM band in the median plane of an active zone. Six ribs, which were segmented for the surface model in Figure 7B, are outlined in gold, and deeper AZM macromolecules lie above them. A secondary docked vesicle (SDV) at the end of the band is connected to an AZM macromolecule (arrow) deep to the nearest rib. At the opposite end of the band there is an undocked vesicle within 30 nm of the presynaptic membrane that is connected to two AZM macromolecules (double arrows). Another undocked vesicle deep to the AZM band is also connected to a macromolecule (triple arrow) arising from the band. **E,F:** Slices made in the median plane of active zones showing pairs of primary docked vesicles directly opposite junctional folds (asterisk) in the postsynaptic plasma membrane of muscle fibers. The portion of the presynaptic membrane immediately associated with the docked vesicles is nearly flat, but the portions beyond the ends of the active zones are irregular (arrows). The pair of vesicles in E are connected to each other by a filamentous macromolecule. Scale bar = 60 nm for A; 75 nm for B,C; 45 nm for D; 55 nm for E; 50 nm for F.

One or two pegs extended directly from each rib to connect to the presynaptic membrane (Figs. 3A–C, 7A–C,E). The sites of peg-presynaptic membrane connections for each AZM band were distributed in paired double rows (Fig. 7E). The linear extent of each double row of peg-membrane connections was similar to that of each double row of membrane macromolecules seen in freeze-fracture replicas of the membrane (Fig. 7D), and for a given pair of double rows of peg-membrane contacts the ends of double rows were not always in register, similar to the paired double rows of membrane macromolecules and paired AZM bands in general (compare Fig. 7D to 7E). Using the moment calculation tool in EM3D (Ress et al., 2004) to measure the centroid spacing of the peg-membrane contact sites we found the mean longitudinal spacing for 48 pegs at three active zones was 18 ± 6 nm (SD), while the transverse spacing was 19 ± 7 nm (SD), which is in good agreement with the longitudinal (17 ± 3 nm) and transverse (19 ± 3 nm) spacing of membrane macromolecules at active zones of mouse NMJs reported by others (Fukuoka et al., 1987). Moreover, at six active zones where we fit a straight line approximating the midline of each double row of peg-membrane contacts the distance between the lines was 63 ± 7 nm (SD), which is in good agreement with the distance between the midlines of double rows of membrane macromolecules at active zones of mouse NMJs as calculated from the measurements of others (Fukuoka et al., 1987; see above). These findings lead to the conclusion that each peg is connected to one of the membrane macromolecules in the double rows, that each macromolecule in the double rows is connected to a peg, and that each of the two pegs associated with a rib is connected to a membrane macromolecule in a different row.

We examined eight secondary docked vesicles for connections to AZM macromolecules. Six were connected to three macromolecules each, two were connected to two macromolecules each. In all cases the connection sites were on the vesicle hemisphere facing the AZM, and the macromolecules arose from the AZM orthogonal and deep to the ribs connected to the nearby primary docked vesicles (Fig. 3D). The distance from the centroid of the nearest macromolecule-vesicle connection site to the presynaptic membrane for eight secondary docked vesicles was 17.8 ± 6.1 nm (SD), which

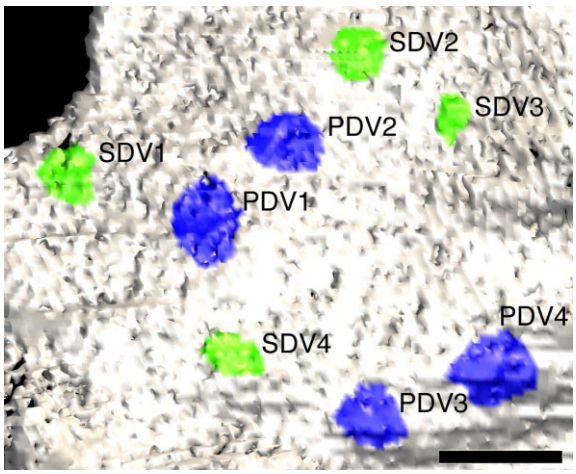

Figure 4.
Areas of direct contact of primary and secondary docked vesicles with the presynaptic membrane. The contact areas of the primary docked vesicles (PDV1-PDV4) and secondary docked vesicles (SDV1-SDV4) were mapped on a surface model of a portion of presynaptic membrane associated with two active zones (shown in Fig. 2F) by assigning colors to the vertices in each contact area. On average the contact areas of the primary docked vesicles (blue) are about twice that of the secondary docked vesicles (green): PDV1 = 230 nm^2, PDV2 = 350 nm^2, PDV3 = 370 nm^2, PDV4 = 260 nm^2, SDV1 = 160 nm^2, SDV2 = 210 nm^2, SDV3 = 80 nm^2, SDV4 = 220 nm^2. Scale bar = 50 nm (as determined by the centroid distance between SDV3 and SDV4).

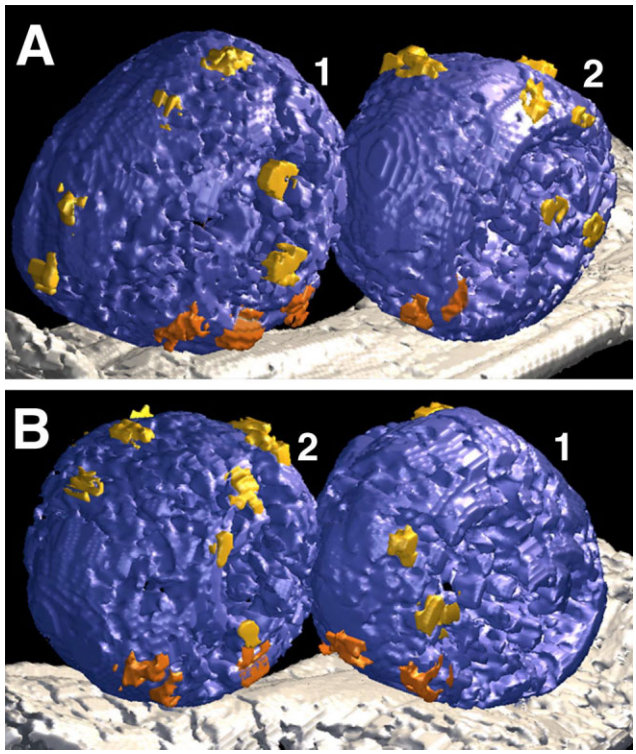

Figure 5.
Distribution of connection sites of active zone material (AZM) filaments on primary docked vesicles. **A,B:** A pair of docked vesicles (1 and 2) at an active zone viewed from each AZM band, showing sites of connection (1 voxel thick) with AZM macromolecules. The connection sites are broadly distributed over the hemispheres. Connection sites formed by ribs, which are within 15 nm of the presynaptic membrane, are dark gold; connection sites formed by AZM macromolecules deep to the ribs are light gold.

was 2-fold greater than the distance from the centroids of rib connection sites on primary docked vesicles to the presynaptic membrane. There were no filaments directly linking AZM filaments connected to the secondary docked vesicles to the presynaptic membrane, such as the pegs which link ribs to the calcium channels in the presynaptic membrane.

We have not yet examined in detail the linkage of the beam-rib-peg assemblies to deeper AZM macromolecules (Fig. 3D). Most, if not all, of the deeper macromolecules seem to be linked to the assemblies near beam-rib junctions.

DISCUSSION

We show by ET that the AZM at active zones of mouse NMJs is arranged in two parallel bands attached to the cytoplasmic surface of the presynaptic membrane. Each band overlies one of the paired double rows of macromolecules that include calcium channels seen in freeze-fracture replicas of the presynaptic membrane (Fukunaga et al., 1983; Fukuoka et al., 1987). Between the bands and parallel to their long axes is a pair of juxtaposed synaptic vesicles contacting the presynaptic membrane. These vesicles, based on the position of vesicle fusion sites in freeze-fracture replicas of the presynaptic membrane at NMJs in rat and on phasic muscle fibers in lizard (Ellisman et al., 1976; Walrond and Reese, 1985), where the active zones are similar to those in mouse, must be docked on the membrane prior to fusion during synaptic activity. There are also vesicles docked on the presynaptic membrane at the ends of the bands, but there is no evidence from freeze-fracture studies that these secondary docked vesicles fuse with the presynaptic membrane during synaptic transmission as do the primary docked vesicles between the bands (Ellisman et al., 1976; Walrond and Reese, 1985).

At active zones of frog NMJs, which have also been studied by ET, there is only a single band of AZM. It can be more than 10 times longer than the AZM bands at the mouse NMJ (e.g., Couteaux and Pécot-Dechavassine, 1970). Paired double rows of macromolecules in the presynaptic membrane underlie the band throughout its length and synaptic vesicles docked on the presynaptic membrane prior to fusion with it during synaptic transmission are in a single row on each side of the band (Couteaux and Pécot-Dechavassine, 1970; Heuser et al., 1974). Thus, the AZM at neuromuscular active zones in mouse is much smaller than that in frog, and it has a bilateral arrangement relative to each primary docked vesicle, while in frog the arrangement of AZM relative to each docked vesicle is unilateral.

Despite the difference in positioning of AZM relative to primary docked vesicles in mouse and to all docked vesicles in frog, the organization of macromolecules in the AZM bands of both species has several similarities. Within 15 nm of the presynaptic membrane, both AZM bands in the mouse's active zone have macromolecular components which, based on their relative orientation and connectivity, correspond to the beams, ribs, and pegs in the frogs' AZM band (Fig. 8). Beams are connected to beams and ribs, ribs are connected to docked vesicles and pegs, and pegs are connected to the

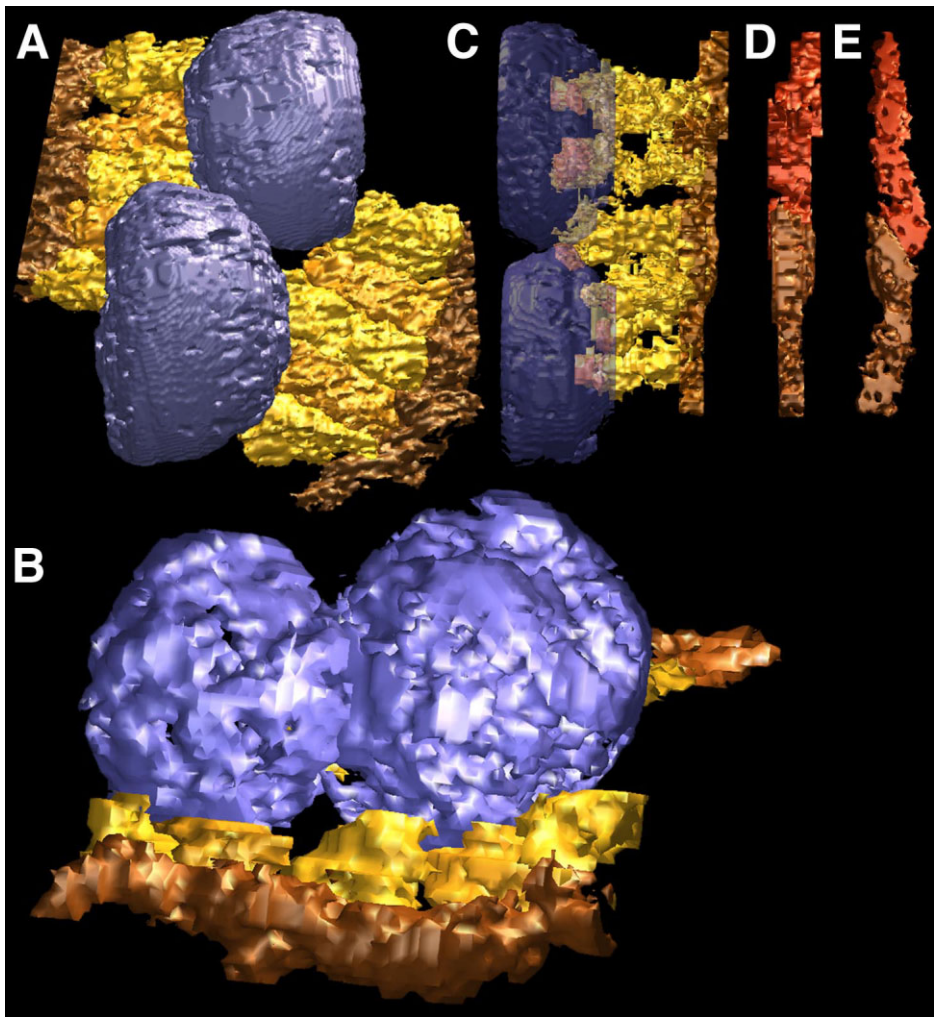

Figure 6.
Connections of beams and ribs. **A–C:** Pairs of primary docked vesicles and the portion of active zone material (AZM) bands within 15 nm of the presynaptic membrane at three different active zones. The AZM's ribs (light gold) are attached in series to both primary docked vesicles and to beams (dark gold). In C, the vesicles were made transparent to show the areas of rib connection sites (orange). **D,E:** Two beams lying in series in C are made discernible with different colors in both the same plane (D) in which they are shown in C and rotated 90° around the long axis (E).

presynaptic membrane in a way indicating that they are linked 1:1 to the membrane macromolecules in the double rows. The number of connections formed by the ends of AZM macromolecules on the vesicles throughout the depth of the AZM bands is also similar between the species. For each primary docked vesicle in mouse there are ≈11 such connection sites, five or six of which are made by ribs. They are nearly evenly distributed between the two hemispheres facing the bands; those connections on a particular hemisphere are formed by macromolecules within the band facing it. For docked vesicles at frog NMJs prepared in the same way as the mouse NMJs used for this study, there were 8.0 ± 1.1 (SD) contact sites per vesicle (n = 12), three or four of which were made by ribs, and they were primarily confined to the vesicle hemisphere facing the AZM band (unpubl. obs.; Harlow et al., 2001). Thus, there is a fractional increase in the number AZM filament contacts on the docked vesicles, including those made by ribs, at mouse active zones. However, the most striking consequence of the species difference in the positioning of AZM relative to docked vesicles observed here is that in mouse the connections to AZM are broadly distributed over two hemispheres, with the connections on each hemisphere from nearly diametrically opposed AZM bands, while in frog they are distributed primarily over a single hemisphere facing a single band.

The orderly linkage of beam-rib-peg assemblies to the double rows of membrane macromolecules and linear arrays of docked vesicles at NMJs of such widely divergent species as frog and mouse leads to the prediction that these assemblies are present at NMJs in other species where the presynaptic membrane has double rows of macromolecules and linear docked vesicles, such as human, rat, and lizard (Rash and Ellisman, 1974; Ellisman et al., 1976; Fukunaga et al., 1982; Walrond and Reese, 1985). Accordingly, at NMJs where the relationship of the double rows of macromolecules to docked vesicles is bilateral, as are those in human, rat, and the junctions on phasic muscle fibers in lizard, the assemblies to-

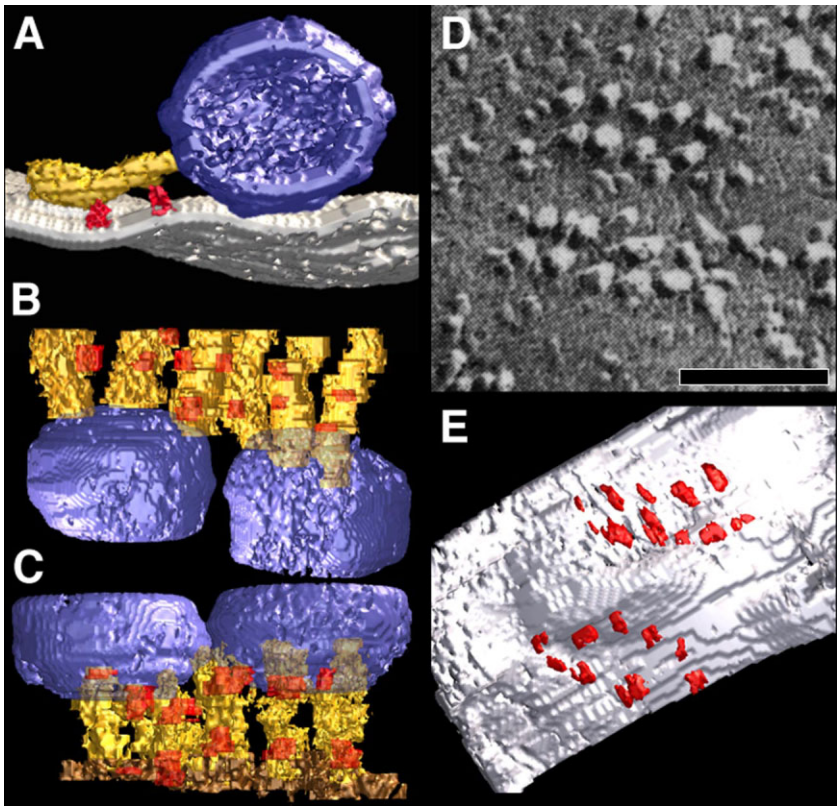

Figure 7.
Connections of pegs to ribs and the presynaptic membrane. **A:** Two pegs (red) extend from a rib to the presynaptic membrane viewed in the transverse plane of an active zone. **B,C:** One or two pegs (red) are connected to each of the several ribs (gold) linked to a pair of primary docked vesicles viewed in the horizontal plane of the active zone. The viewpoint is deep to the ribs, which have been made transparent to show the contact sites of the pegs. **D:** Freeze-fracture replica from the presynaptic membrane of a mouse neuromuscular junction showing paired double rows of membrane macromolecules (from fig. 2, Fukuoka et al., 1987. Annals of Neurology 22:193–199, Copyright © 1987, Wiley-Blackwell, reproduced by permission). **E:** A surface model of the presynaptic membrane at an active zone with attached pegs viewed in the same plane and at the same scale as the freeze-fracture replica from the presynaptic membrane in D. The frequency and distribution of peg connection sites on the presynaptic membrane is similar to the frequency and distribution of macromolecules in the freeze-fracture replica of the membrane. Scale bar = 50 nm in D (calculated from reported magnification).

gether with deeper AZM macromolecules would be in a pair of bands bilateral to the docked vesicles, as in mouse. At junctions where the relationship of the double row of membrane macromolecules to docked vesicles is unilateral, as at the junctions on the tonic muscle fibers of the lizard, the arrangement of the AZM relative to docked vesicles would be in a single band unilateral to docked vesicles, as in frog. Whether or not AZM contains structures identical to the beams, ribs, and pegs at the many other synaptic types throughout vertebrate and invertebrate nervous systems, where the arrangement of membrane macromolecules and docked vesicles is not linear and positioning of AZM relative to docked vesicles is more complex than at NMJs (Heuser and Reese, 1981; Waldrond et al., 1993; Zhai and Bellen, 2004; Prokop and Meinertzhagen, 2006; Zampighi et al., 2008), it is reasonable to expect, based on similarities in active zone function, that in general AZM will have an orderly arrangement of macromolecules that link it to calcium channels in the presynaptic membrane and to docked vesicles.

The associations of AZM macromolecules at active zones of the mouse NMJ are consistent with the hypothesis that the AZM helps dock synaptic vesicles on the presynaptic membrane, anchor the channels in the membrane, and maintain the vesicles and channels at a particular distance from each other (Harlow et al., 2001). The AZM is also likely to be involved in the fusion of the primary docked vesicles with the presynaptic membrane (Harlow et al., 2001). Thus, its macromolecules are expected to include many of the proteins, e.g., SNAREs, shown by biochemical molecular biology to be involved in vesicle docking and fusion at synapses in general (Südhof, 2004). Because of the amount of its molecular mass, the cytoplasmic portion of the calcium channel itself may compose much of a peg and perhaps part of a rib (Harlow et al., 2001). The bilateral arrangement of AZM bands relative to primary docked vesicles and their connections to the vesicle hemispheres facing them may favor more efficient vesicle docking and/or fusion than in cases where the contacts are unilaterally distributed, as in frog. We show here that the size of the area of contact between the membrane of primary docked vesicles and the presynaptic membrane at mouse NMJs is 395 ± 40 nm^2 (SEM, n = 12). Similar measurements made at frog NMJs prepared in the same way as those in mouse show that, while the average diameter of the docked vesicles is similar to that of the primary docked vesicles at mouse neuromuscular junctions (54.8 ± 5.3 nm [SD] vs. 55.6 ±

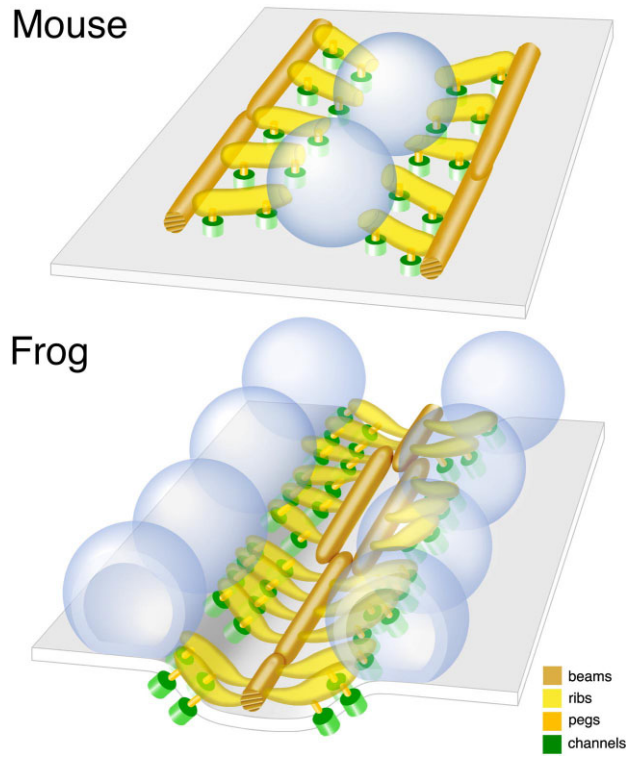

Figure 8.
Comparison of the arrangement of beams, ribs, and pegs at active zones of mouse and frog neuromuscular junctions. Scheme for frog is from Ress et al. (2004). Structure 12:1763–1774, Copyright © 2004, Elsevier Ltd., reproduced by permission.

3.3 nm [SD]), the size of the vesicle-membrane contact area is 299 ± 21 nm^2 (SEM, n = 42; unpubl. obs.). Thus, in terms of the size of the vesicle membrane-presynaptic membrane contact area, the docking efficacy of the mouse active zone is significantly greater than that of the frog. Moreover, the probability of a primary docked vesicle fusing with the presynaptic membrane at the mouse NMJ is also likely to be greater than at frog NMJs. Based on the observations that the area of the presynaptic membrane directly facing the muscle fiber at mouse neuromuscular junctions is 80–100 μm^2 (Fahim et al., 1983) and there are ≈2.5 active zones per μm^2 of presynaptic membrane junction (Fukunaga et al., 1983; Fukuoka et al., 1987), we predict there are ≈225 active zones per junction. Based on quantal content of the endplate potential at mouse NMJs, it has been estimated that about 50 synaptic vesicles fuse with the presynaptic membrane at a junction after arrival of a nerve impulse (e.g., Banker et al., 1983). Thus, our observation that there are only two primary docked vesicles per active zone leads to the conclusion that there are about 450 primary docked vesicles per NMJ, and that there is about a 10% probability of a primary docked vesicle fusing with the membrane during such activity. This agrees with similar but less direct probability estimates (Walrond and Reese, 1985; Rash et al., 1988) for evoked vesicle fusion at active zones of NMJs in human and rat muscles and on phasic muscle fibers in lizard muscles (≈6%), where we predict that the AZM like the presynaptic membrane macromolecules at the active zones has a bilateral distribution relative to docked vesicles, and it is 10-fold greater than probability estimates for NMJs in frog and on tonic muscle fibers of the lizard (Walrond and Reese, 1985; Rash et al., 1988), where the AZM and membrane macromolecules have a unilateral arrangement relative to the docked vesicles. The increased probability of vesicle fusion at active zones that have a bilateral distribution of calcium channels may be a function of an increased number of calcium sources in the vicinity of each vesicle for triggering fusion (Walrond and Reese, 1985), but if the ribs and/or other macromolecules in the AZM contain proteins that exert either a constant or calcium triggered force on the membrane of docked vesicles essential to the vesicles' fusion with the presynaptic membrane, bilateral connections of such macromolecules to a docked vesicle may also favor an increased probability of fusion over unilateral connections. We observed that the curvature of the docked vesicles at the mouse active zone appears distorted at sites of contact with the ribs in a way that indicates force on the membrane of docked vesicles in the direction of the ribs at the time of fixation.

The area of contact of secondary docked vesicles with the presynaptic membrane at the ends of AZM bands is, on average, one-half that of primary docked vesicles between the bands. Moreover, the secondary docked vesicles are connected to the AZM by one-fourth as many AZM macromolecules as primary docked vesicles, the macromolecules arise from the AZM orthogonal and deep to the ribs that are attached to the nearby primary docked vesicles, and the macromolecules have no obvious connection to calcium channels as do ribs via pegs. These differences between the associations of secondary and primary docked vesicles together with the absence of evidence that secondary docked vesicles fuse with the presynaptic membrane when fusion of the primary docked vesicles is evoked by exposure to high potassium concentrations, as discussed above, raise the problem of whether the secondary docked vesicles are manifestations of an early stage in the recycling of vesicle membrane from the presynaptic membrane after the primary docked vesicles have fused with it during synaptic transmission. At NMJs the membrane of vesicles that have fused with the presynaptic membrane can move away from the fusion site before it is retrieved from the presynaptic membrane to form a vesicle that is capable of fusing again (Heuser and Reese, 1973, 1981; Miller and Heuser, 1984). At NMJs on phasic muscle fibers in the snake, where the arrangement of macromolecules in the presynaptic membrane at active zones is similar to that in mammals, the retrieval has been shown by fluorescence microscope histochemistry to preferentially occur immediately adjacent to the active zones (Teng et al., 1999). We show at mouse NMJs that there are deep invaginations in the presynaptic membrane selectively localized to the region just beyond the ends of the active zones, indicating that this region of the presynaptic membrane differs from elsewhere in a way that might be expected if it were involved in the recycling of vesicle membrane. We also show that at the ends of those AZM bands lacking secondary docked vesicles, there are vesicles selectively located within 30 nm of the membrane connected to the bands in a way similar to that of the secondary docked vesicles. Altogether, these findings are consistent with the possibility that secondary docked vesicles are newly retrieved from the presynaptic membrane and destined to move away from the membrane in association with the AZM. Such associations might favor subsequent docking of

these vesicles on the presynaptic membrane between the bands over those vesicles deeper within the terminal and, thus, help account for a preferential use of newly retrieved vesicles during synaptic transmission, as has been shown at neuromuscular junctions and other synapses by other technology (e.g., Rizzoli and Betz, 2005).

LITERATURE CITED

Angaut-Petit D, Molgo J, Connold AL, Faille L. 1987. The *levator auris* longus muscle of the mouse: a convenient preparation for studies of short- and long-term presynaptic effects of drugs or toxins. Neurosci Lett 82:83–88.

Arfken G. 1985. Eigenvectors, eigenvalues. In: Mathematical methods for physicists, 3rd ed. Orlando, FL: Academic Press. p 229–237.

Banker BQ, Kelly SS, Robbins N. 1983. Neuromuscular transmission and correlative morphology in young and old mice. J Physiol 339:355–375.

Couteaux R, Pécot-Dechavassine M. 1970. Vésicules synaptiques et poches au niveau des "zones actives" de la junction neuromusculaire. Compt Rend 271:2346–2349.

Cristina VI, Wright ER, Benjamin J, Tivol WF, Dias DP, Murphy GE, Morrison RC, Heymann JB, Jensen GJ. 2005. A "flip-flop" rotation stage for routine dual-axis electron cryotomography. J Struct Biol 151:288–297.

Dresbach T, Qualmann B, Kessels MM, Garner CC, Gundelfinger ED. 2001. The presynaptic cytomatrix of brain synapses. Cell Mol Life Sci 58:94–116.

Ellisman MH, Rash JE, Staehelin LA, Porter KR. 1976. Studies of excitable membranes II. A comparison of specializations at neuromuscular junctions and nonjunctional sarcolemmas of mammalian fast and slow twitch muscle fibers. J Cell Biol 68:752–774.

Fahim MA, Holley JA, Robbins N. 1983. Scanning and light microscopic study of age changes at a neuromuscular junction in the mouse. J Neurocytol 12:13–25.

Fukunaga H, Engel AG, Osame M, Lambert EH. 1982. Paucity and disorganization of presynaptic membrane active zones in the Lambert-Eaton myasthenic syndrome. Muscle Nerve 5:686–697.

Fukunaga H, Engel AG, Lang B, Newsome-Davis J, Vincent A. 1983. Passive transfer of Lambert-Eaton myasthenic syndrome with IgG from man to mouse depletes the presynaptic membrane active zones. Proc Natl Acad Sci U S A 80:7636–7640.

Fukuoka T, Engel AG, Lang B, Newsome-Davis J, Prior C, Wray DW. 1987. Lambert-Eaton myasthenic syndrome: I. Early morphological effects of IgG on the presynaptic membrane active zones. Ann Neurol 22:193–199.

Gray EG. 1966. Problems of interpreting the fine structure of vertebrate and invertebrate synapses. Gen Exp Zool 2:139–170.

Harlow ML, Ress D, Stoschek A, Marshall RM, McMahan UJ. 2001. The architecture of active zone material at the frog's neuromuscular junction. Nature 409:479–484.

Heuser JE, Reese TS. 1973. Evidence for recycling of synaptic vesicle membrane during transmitter release at the frog neuromuscular junction. J Cell Biol 57:315–344.

Heuser JE, Reese TS. 1977. The structure of synapses. In: Handbook of physiology, vol. I. The nervous system. Bethesda, MD: American Physiological Society. p 261–294.

Heuser JE, Reese TS. 1981. Structural changes after transmitter release at the frog neuromuscular junction. J Cell Biol 88:564–580.

Heuser JE, Reese TS, Landis DM. 1974. Functional changes in frog neuromuscular junctions studied with freeze-fracture. J Neurocytol 3:109–131.

Hirokawa N, Sobue K, Kanda K, Harada A, Yorifuji H. 1989. The cytoskeletal architecture of the presynaptic terminal and molecular structure of synapsin 1. J Cell Biol 108:111–106.

Katz B. 1969. The release of neural transmitter substances. Springfield, IL: Thomas.

Landis DM, Hall AK, Weinstein LA, Reese TS. 1988. The organization of cytoplasm at the presynaptic active zone of a central nervous system synapse. Neuron 1:201–209.

Lang B, Newson-Davis J, Peers C, Prior C, Wray DW. 1987. The effect of myasthenic syndrome antibody on presynaptic calcium channels in the mouse. J Physiol 390:257–270.

Miller TM, Heuser JE. 1984. Endocytosis of synaptic vesicle membrane at the frog neuromuscular junction. J Cell Biol 98:685–698.

Nagel A, Engel AG, Lang B, Newsome-Davis J, Fukuoka T. 1988. Lambert-Eaton myasthenic syndrome IgG depletes presynaptic membrane active zone particles by antigenic modulation. Ann Neurol 24:552–558.

Pawson PA, Grinnell AD, Wolowske B. 1998. Quantitative freeze-fracture analysis of the frog neuromuscular junction synapse. I. Naturally occurring variability in active zone structure. J Neurocytol 27:361–377.

Pearson K. 1901. On lines and planes of closest fit to systems of points in space. Philos Mag 2:559–572.

Penczek P, Marko M, Buttle K, Frank J. 1995. Double-tilt electron tomography. Ultramicroscopy 60:393–410.

Peters A, Palay SL, Webster H deF. 1991. The fine structure of the nervous system. Oxford: Oxford Press. p 198–203.

Prokop A, Meinertzhagen IA. 2006. Development and structure of synaptic contacts in *Drosophila*. Semin Cell Dev Biol 17:20–30.

Rash JE, Ellisman ME. 1974. Studies of excitable membranes I. Macromolecular specializations of the neuromuscular junction and the nonjunctional sarcolemma. J Cell Biol 63:567–586.

Rash JE, Walrond JP, Morita M. 1988. Structural and functional correlates of synaptic transmission in the vertebrate neuromuscular junction. J Electron Microsc Tech 10:153–185.

Ress D, Harlow M, Schwarz M, Marshall RM, McMahan UJ. 1999. Automatic acquisition of fiducial markers and alignment of images in tilt series for electron tomography. J Elect Microsc 48:277–287.

Ress D, Harlow ML, Marshall RM, McMahan UJ. 2003. Optimization methods for isodensity surface models obtained with electron microscope tomography data. Engineering in Medicine and Biology Society, 2003. Proceedings of the 25th Annual Conference of the IEEE 1:774–77.

Ress DB, Harlow ML, Marshall RM, McMahan UJ. 2004. Methods for generating high-resolution structural models from electron microscope tomography data. Structure 12:1763–1774.

Rizzoli SO, Betz WJ. 2005. Synaptic vesicle pools. Nat Rev Neurosci 6:57–69.

Roberts WM, Jacobs RA, Hudspeth AJ. 1990. Colocalization of ion channels involved in frequency selectivity and synaptic transmission at presynaptic active zones of hair cells. J Neurosci 10:3664–3684.

Robitaille R, Garcia ML, Kaczorowski GJ, Charlton MP. 1993. Functional colocalization of calcium and calcium-gated potassium channels in control of transmitter release. Neuron 11:645–655.

Siksou L, Rostaing P, Lechaire J, Boudier T, Ohtsuka T, Fejtova A, Kao H, Greengard P, Gundelfinger ED, Triller A, Marty S. 2007. Three-dimensional architecture of terminal cytomatrix. J. Neurosci 27:6868–6877.

Sosinsky GE, Crum J, Jones YZ, Lanman J, Smarr B, Terada M, Martone ME, Deerinck TJ, Johnson JE, Ellisman MH. 2008. The combination of chemical fixation procedures with high pressure freezing and freeze substitution preserves highly labile tissue ultrastructure for electron tomography applications. J Struct Biol 161:359–371.

Südhof TC. 2004. The synaptic vesicle cycle. Annu Rev Neurosci 27:509–547.

Takamori S, Holt M, Stenius K, et al. 2006. Molecular anatomy of a trafficking organelle. Cell 127:831–846.

Teng H, Cole JC, Roberts RL, Wilkinson RS. 1999. Endocytic active zones: hot spots for endocytosis in vertebrate neuromuscular terminals. J Neurosci 19:4855–4866.

Walrond JP, Reese TS. 1985. Structure of axon terminals and active zones at synapses on lizard twitch and tonic muscle fibers. J Neurosci 5:1118–1131.

Walrond JP, Govind CK, Huestis SE. 1993. Two structural adaptations for regulating transmitter release at lobster neuromuscular synapses. J Neurosci 13:4831–4845.

Zampighi GA, Zampighi LM, Fain N, Lanzavecchia S, Simon SA, Wright EM. 2006. Conical electron tomography of a chemical synapse: vesicles docked to the active zone are hemi-fused. Biophys J 91:2910–2918.

Zampighi GA, Fain N, Zampighi LM, Cantele, F, Lanzavecchia S, Wright EM. 2008. Conical electron tomography of a chemical synapse: polyhedral cages dock vesicles to the active zone. J Neurosci 28:4151–4160.

Zhai RG, Bellen HJ. 2004. The architecture of the active zone in the presynaptic nerve terminal. Physiology 19:262–270.

Zheng QS, Braunfeld MB, Sedat JW, Agard DA. 2004. An improved strategy for automated electron microscopic tomography. J Struct Biol 147:91–101.